Journal of Quantitative Spectroscopy & Radiative Transfer 330 (2025) 109265

Contents lists available at ScienceDirect

Journal of Quantitative Spectroscopy and Radiative Transfer

journal homepage: www.elsevier.com/locate/jqsrt

# The j and k dependencies of $N_2$-, $O_2$-, and air-broadened halfwidths of the $CH_3CN$ molecule

Q. Ma [a,*], C. Boulet [b]

[a] NASA/Goddard Institute for Space Studies and Department of Applied Physics and Applied Mathematics, Columbia University, 2880 Broadway, New York, NY 10025, USA

[b] Institut des Sciences Moléculaires d'Orsay (ISMO), CNRS, Université Paris-Saclay, Bât. 520, Campus d'Orsay 91405, Orsay-Cedex, France

ARTICLE INFO

*Keywords:*
Methyl Cyanide N2-
O2-
And air-broadened halfwidths of CH3CN line coupling and line mixing temperature exponents semi-classical line shape theory

ABSTRACT

The $N_2$-, $O_2$, and air-broadened halfwidths of $CH_3CN$ lines in the parallel $\nu_4$ band have been calculated, along with the relaxation matrices W. These calculations employ our modified and refined versions of the Robert-Bonamy formalism and use all potential parameters from the literature without adjustments. Extensive comparisons between the predicted $N_2$-broadened halfwidths in the qR and qP branches from the models at $T = 296$ K and experimental measurements are presented, showing that our latest model very closely matches the measurements. For the qQ branch, where measurements are unavailable, we compare our $N_2$-broadened halfwidths with the converted air-broadened data from HITRAN 2008, obtaining similarly good agreement. The variation in the j and k dependencies of the $N_2$-broadened halfwidths is discussed in detail. Additionally, the theoretically determined conversion factor from $N_2$- to air-broadening is provided. Finally, based on our theoretical calculations of $N_2$-broadened halfwidths of the qR(j,3) lines at five different temperatures, ranging from 250 K to 350 K, the temperature exponent $N$ is determined and its dependence on j is analyzed.

## 1. Introduction

Methyl Cyanide ($CH_3CN$) is recognized as a long-living pollutant in the Earth's atmosphere and is also of significant astrophysical interest, having been also detected in planetary atmospheres, such as that of Titan, as well as in the interstellar medium and comets [1–3]. Therefore, precise knowledge of its spectroscopic parameters (i.e., line frequencies, intensities, pressure broadened halfwidths and induced shifts, temperature exponents, and appropriate lineshape profiles) is essential for developing accurate remote sensing models. In this work, we focus on the $CH_3CN$ line broadening by $N_2$ and $O_2$, which are primary components in Earth's atmosphere. $N_2$ broadening is particularly important in Titan's atmosphere, where the $N_2$ abundance is around 98.4 %.

Given this interest, several line broadening measurements have been done, with a detailed review available in Ref. [1–3]. Most of these studies focused on only a few lines in the pure rotational band [1,4]. However, in 2008, Rinsland et al. [3] published $N_2$-broadening data for about 700 lines in both the qR and qP branches of the parallel $\nu_4$ band at room temperature, providing a valuable resource for developing the broadening coefficients adopted by the HITRAN 2008 database [5].

From a theoretical perspective, the most recent calculation of $N_2$-broadening halfwidths for $CH_3CN$ [2] applied Bykov's semi-empirical approach [6] for calculating line broadening coefficients with their temperature dependence. Remind that this method employs analytical Anderson-type expressions for halfwidth, corrected by an empirical factor with a few parameters to account for real trajectory curvature, vibrational effects, and corrections to the scattering matrix. Once the model parameters are calibrated using some experimental halfwidths, extensive calculations can be performed across a wide ranges of j and k values required by spectroscopic databases.

Previously, using the Robert-Bonamy (RB) formalism [7], Colmont et al. [1] conducted a purely theoretical calculation of $N_2$-broadened halfwidths for $CH_3CN$. Unfortunately, their efforts were unsuccessful, leading them to conclude that for molecules with a large dipole and/or quadrupole moment, the RB method would results in a significantly overestimation. It is worth noting that the RB method, developed in 1979, is based on the isolated line approximation, in which the matrix elements of the operator $exp(-S_2)$ are replaced by the exponential of the matrix elements of $-S_2$. In other words, exponential of the operator is assumed to behave like as an ordinary function. However, as previously noted by Cherkasov in 1976 [8] and also Buffa and Tarrini in 1977 [9], the $-S_2$ operator is not diagonal in the linespace. As a result, this

* Corresponding author.
*E-mail address:* qm2@columbia.edu (Q. Ma).

https://doi.org/10.1016/j.jqsrt.2024.109265
Received 10 October 2024; Received in revised form 6 November 2024; Accepted 6 November 2024
Available online 8 November 2024

replacement is not valid, which severely limits the reliability of the RB formalism. The poor performance of the RB method was also demonstrated in our recent studies of the $CH_3X$-$N_2$ systems [10–14].

An alternative approach, which we call the Refined Robert Bonamy (RRB) model, has been developed by us [15,16]. In this model, we used the cumulant expansion instead of the Linked-Cluster theorem employed by Robert and Bonamy. This modification not only corrects a subtle derivation error in the RB method, but also dramatically reduces the matrix size of $-S_2$. This reduction is a crucial advancement, as it allows to remove the isolated line approximation and to accurately evaluate the matrix elements of $exp(-S_2)$. In addition, the entire relaxation matrix W can be calculated based on the potential energy surfaces between the two interacting molecules. As a result, this approach enables the treatment of line mixing effects, which the RB formalism had previously failed to address.

Finally, we would like to explain the terminology related to line coupling (LC) and line mixing (LM). These terms are used to describe effects from the non-diagonality of $exp(-S_2)$ and of the resolvent operator $(\omega - L_0 - iPW)^{-1}$respectively. By accounting for LM, the calculated "effective" halfwidths can be further reduced, as discussed in our recent papers devoted to $N_2$-broadening of $CH_3X$-species [10–14].

For symmetric tops with k-degeneracy, the original eigenfunctions are inadequate for describing a symmetric-top rotor. Instead, a more proper approach involves using symmetric and asymmetric combinations of the two rotational functions with k and -k [17]. As a result, a given transition $j_f\, k \leftarrow j_i\, k$ should be treated as a doublet, except when $k = 0$ [8]. Then, the two components of each doublet can be coupled through the LM process. For degenerate doublets (i.e. those not resolved by any hyperfine splitting), LM can significantly reduce the halfwidths of the doublet. As shown in our previous works, this feature provides a strong explanation for the LM effects observed in the halfwidths of $N_2$-broadened $CH_3X$.

The manuscript is arranged as follows. Section II provides a brief overview of the theoretical model. Sec. III presents the theoretically calculated $N_2$- and $O_2$-broadened halfwidths of $CH_3CN$ lines in the $\nu_4$ band, with comparisons to experimental measurements and the values listed in HITRAN 2008. A detailed analysis of the temperature dependence of the halfwidths is also included. Concluding remarks are given in Sec. IV.

## 2. Theory

### 2.1. A short background

Within the binary collision and impact approximations and using a symmetrized form, the spectral density can be written as [16,18],

$$F(\omega) = \frac{1}{\pi} Im \sum_{n,l} d_l \sqrt{\rho_l} \left\langle l \left| \frac{1}{\omega - L_0 - iPW} \right| n \right\rangle \sqrt{\rho_n} d_n \tag{1}$$

Here $|n\rangle \equiv |j_f k_f \varepsilon_f; j_i k_i \varepsilon_i\rangle$ is the Liouville vector associated to the transition $j_f k_f \varepsilon_f \leftarrow j_i k_i \varepsilon_i$. A background of this basis set applicable for symmetric tops is given in Sec. II and Appendix of Ref. [19]. In Eq. (1), $\rho_n = \frac{\exp(-\beta E_n)}{Z}$ represents matrix elements of the density operator without consideration for magnetic degeneracy. The term $Z$ denotes the partition function, $E_n = E(v_i j_i k_i \varepsilon_i)$ is the initial energy of transition. In addition, $d_n$ stands for the associated transition dipole operator and $L_0$ is the diagonal matrix of transition frequency. Finally, $P$ is the bath pressure and $W$ is the symmetrized relaxation matrix. The correspondence between the symmetrized form and the "usual" unsymmetrized one is recalled in Appendix A of Ref. [18].

We do not repeat the detailed development processes of our formalisms here. Readers are referred to our earlier works ($CH_3D$-$N_2$) [12] for this information. Instead, we only briefly explain the key physical advancements. The modified Robert-Bonamy (MRB) method is an earlier version where a subtle derivation error in the RB formalism was corrected, but the isolated line approximation was still applied [15]. Within the MRB method, halfwidths $\gamma_{fi}$ can be calculated using the following formula:

$$\gamma_{fi} = \frac{n_b \bar{\nu}}{2\pi c} \int_{r_{c,min}}^{+\infty} 2\pi b \left(\frac{db}{dr_c}\right) \left\{1 - e^{-\langle fi|S_2|fi\rangle}\right\} dr_c, \tag{2}$$

where $n_b$ is the number density of the bath molecules, $\bar{\nu}$ is the mean relative speed, $b$ is the impact parameter, and $r_c$ is the closest distance for a given trajectory. Meanwhile, in Eq. (2) an average over the collisional kinetic energy is replaced by the mean relative speed $\bar{\nu}$.

The subsequent version is the refined Robert-Bonamy (RRB) method, in which the invalid isolated line approximation is removed, and the effects from line coupling (LC) are considered [16]. The RRB method allows for the calculation of the entire relaxation matrix W, whose diagonal elements correspond to the calculated halfwidths. The expression for W is given as follows:

$$W_{f'i',fi} = \frac{n_b \bar{\nu}}{2\pi c} \int_{r_{c,min}}^{+\infty} 2\pi b \left(\frac{db}{dr_c}\right) \left\{\delta_{i'i}\delta_{f'f} - \langle f'i'|e^{-S_2(r_c)}|fi\rangle\right\} dr_c. \tag{3}$$

Our most advanced formalism is the RRB with line mixing (LM) method. This method further accounts for the effect from LM due to the non-diagonality of $L_0 - iPW$ in the resolvent operator $(\omega - L_0 - iPW)^{-1}$. At relative low perturber's pressures in the experiment [3], most of the doublets are isolated and the size of their line space is limited to $2 \times 2$. By applying Ben Reuven's method [20], the "effective" halfwidth of an isolated doublet is the sum of the diagonal and off-diagonal elements. Using simple notations 1 and 2 representing the two components, we have $W(1,1) \equiv W_{f_1 i_1 f_1 i_1} = W_{f_2 i_2 f_2 i_2}$ and $W(1,2) \equiv W_{f_1 i_1 f_2 i_2}$. The "effective" halfwidth of a doublet then becomes $W(1,1) + W(1,2)$. Since $W(1,2)$ is negative, $W(1,1) + W(1,2)$ is smaller than $W(1,1)$. As demonstrated later, this effect can dramatically reduce the calculated halfwidths.

### 2.2. The intermolecular potential

For systems consisting of a symmetric-top molecule and a linear one, the potential can be expressed in terms of a spherical tensor expansion as (cf. Eq. (4) of [21] and references therein),

$$V\left(\vec{R}(t)\right) = \sum_{L_1 K_1 L_2 L} U(L_1 L_2 L; K_1 K_2 = 0; R(t)) \times \sum_{\mu_1 \mu_2 M} C(L_1 L_2 L, \mu_1 \mu_2 M) D^{L_1 *}_{\mu_1 K_1}(\Omega_1) D^{L_2 *}_{\mu_2 0}(\Omega_2) Y^*_{LM}(\Omega(t)), \tag{4}$$

where $\Omega_1$,$\Omega_2$ and $\Omega(t)$ define respectively the orientation of molecule 1, of molecule 2, and of the vector between their two centers of mass.

The anisotropic part of the models for $CH_3CN$—$N_2$ and $CH_3CN$—$O_2$ includes all the long range interactions, including electrostatic, induction, and dispersion forces, with $L_1$, $L_2 \leq 2$ (refer to Eq. (7) of Ref. [1]). All molecular parameters, as listed in Table 1, are taken from sources available in the literature, not adjusted to fit the data. For $CH_3CN$ and $N_2$, the interaction parameters are exactly those given in Table 4 of Ref. [1], except for two corrections: the value of −1.30 (referred by these authors to as "a rather low value of the quadrupole moment of $N_2$" in Ref. [1]) has been replaced by the more typical value −1.40, and the sign error in the Q parameter for $CH_3CN$ has been corrected. Meanwhile, the

**Table 1**
Molecular parameter and anisotropic interaction parameters.

| | M (g mol$^{-1}$) | U (eV) | α (Å$^3$) | γ | d (D) | Q (DÅ) |
|---|---|---|---|---|---|---|
| $CH_3CN$ | 41.0519 | 12.20 | 4.134 | 0.164 | 3.913 | −1.80 |
| $N_2$ | 28.0134 | 15.58 | 1.74 | 0.137 | 0 | −1.40 |
| $O_2$ | 31.9988 | 12.0697 | 1.5689 | 0.233 | 0 | −0.40 |

parameters for $O_2$ are taken from Table 1 of Ref. [22]. We note that no further adjustments were made to fit the measurements.

Fig. 1(a) and 1(b) illustrate the various components $U(L_1L_2L; 00; R)$ of these potential models. Given the large dipole and quadrupole moments of $CH_3CN$, we are confident that these potential models are adequate for describing the interactions for these two molecular systems. As shown in Fig. 1(a), the dominant component for $CH_3CN$—$N_2$ is (123) (red), which primarily represents the dipole-quadrupole interaction between the $CH_3CN$ and $N_2$ molecules. The next important three are (101) (green), (202) (blue), and (224) (black). The remaining components (i.e., (220) (cyan), (121) (magenta), and (222) (yellow)) are negligible. In fact, our numerical calculations demonstrate that the largest contributor to the pressure broadening is the (123) component. Contributions from other components are negligible.

With respect to the interaction between $CH_3CN$ and $O_2$, as shown in Fig. 1(b), the dominant component is also (123). However, because the quadrupole of $O_2$ is significantly smaller than that of $N_2$, this interaction is much weaker than the $CH_3CN$—$N_2$ interaction. Therefore, $O_2$-broadened halfwidths are expected to be significantly smaller that $N_2$-broadened ones.

In Table 1, d and Q are the dipole and quadrupole moments, respectively. α and γ are the isotropic polarizability and the anisotropy of polarizability. U is the first ionization energy. An explicit expression for these anisotropic interactions is provided in Eq. (7) of Ref. [1].

As usual, we assume that the collisional trajectories are determined solely by the isotropic part of the potential. In this work, we use the Lennard-Jones model with parameters provided in Table 2. For molecular systems, the LJ parameters are derived from related molecules using usual combination rules.

In Table 2, all parameters are taken directly from the literature [1, 23] without any adjustments.

Finally, the energy levels of $CH_3CN$ were calculated with the parameters given in Ref. [1].

### 2.3. Construction of the linespace

Since all the components of the potential correspond to $K_1 = 0$, the collisional selection rule is $\Delta k = 0$, which is the same as the radiative selection rule. Consequently, the whole linespace for the $\nu_4$ band of $CH_3CN$ can be divided into uncoupled sub-blocks, since the line coupling does not occur between two lines with different initial k values. Moreover, based on our experience, inter-branch couplings can be reasonably neglected [24]. Then, the linespace with a given k can be further divided into the qR(j,k), qQ(j,k), and qP(j,k) branches, where q indicates $\Delta k = 0$ and R, Q, and P correspond to $\Delta j = 1$, 0, −1, respectively.

**Table 2**
The LJ parameters for the molecules and molecular systems.

| | CH3CN | $N_2$ | CH3CN—$N_2$ | $O_2$ | CH3CN—$O_2$ |
|---|---|---|---|---|---|
| σ (Å) | 4.452 | 3.816 | 4.134 | 3.507 | 3.9795 |
| ε (K) | 60.14 | 92.91 | 74.7503 | 117.69 | 84.1301 |

### 2.4. Line coupling strength factor

As explained in our previous study, within a doublet the LC effect is mainly determined by the coupling strength factor (CSF) defined by

$$(-1)^{L_1}\left(2j_f+1\right)(2j_i+1)\ W\left(j_ij_fj_ij_f,\ 1L_1\right)D^P\left(\varepsilon_i'j_ik_i,\ \varepsilon_ij_ik_i;\ L_10\right)D^P\left(\varepsilon_f'j_fk_f,\ \varepsilon_fj_fk_f;\ L_10\right), \tag{5}$$

where $W(j_ij_fj_ij_f1L_1)$ is the Wigner 6j symbol and the $D^P$ matrix is defined in Eq. A(3) of Ref. [21]. Since both the $CH_3CN$–$N_2$ and $CH_3CN$–$O_2$ systems are characterized by $L_1 = 1$ as their dominant potential component, one can focus attention on the CSF term with $L_1 = 1$.

In Fig. 2(a) and 2(b), we present the magnitudes of CSF(1) for doublets of the qR(j,k) and qQ(j,k) lines, where k ranges from 1 to 9 and j ranges from its minimum k up to 46. The figure demonstrates a well-defined pattern in the variation of CSF(1). It is noticeable that as k increases, the magnitudes of CSF(1) also increase. Meanwhile, with an increase in j, the magnitudes of CSF(1) decrease. Therefore, one can expect the effect of LM to increase as k increases, and to decrease as j increases. This expectation is confirmed by our calculated halfwidths, as shown later.

Furthermore, as demonstrated in Fig. 2(a) and 2(b), the magnitudes of CSF(1) at a given k value in the qQ branch are larger than those in the

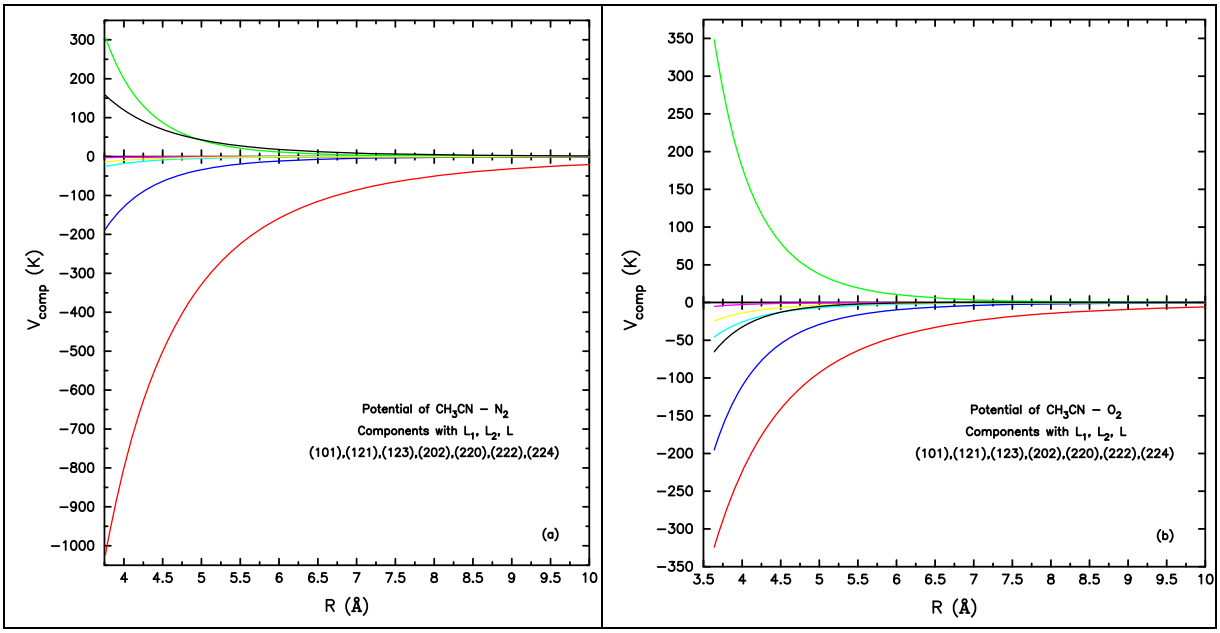


**Fig. 1.** Spherical components, labeled by $(L_1L_2L)$, for the interaction of $CH_3CN$ - $N_2$ and $CH_3CN$ - $O_2$, are shown in Figs. (a) and (b), respectively. With the current cutoff, there are seven components: (101), (121), (123), (202), (220), (222), and (224), each represented by solid curves in seven different colors: green, magenta, red, blue, cyan, yellow, and black.

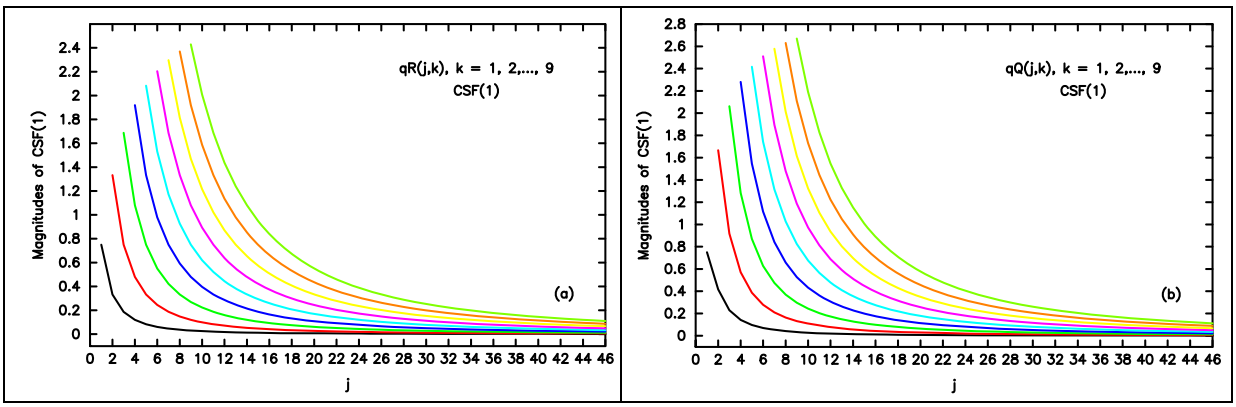


**Fig. 2.** Magnitudes of the coupling strength factor (CSF) with $L_1 = 1$ for the qR and qQ branches where k ranges from 1 to 9 and j ranges from k to 46. They are presented by solid lines in (a) and (b), respectively. Nine different colors are used to distinguish nine different k values. The lowest curve is $k = 1$ and the highest one is $k = 9$.

qR branch. Consequently, one can expect that the effect from LC will be stronger in the qQ branch compared to the qR branch. This expectation is also confirmed by our calculated halfwidths, as shown later.

### 2.5. Symmetry property

Due to the very weak vibrational dependence of both the rotational constants governing collisional transitions and the average values of the molecular parameters in the initial and final vibrational levels, some symmetry properties can be established from theoretical considerations. In this study, a relationship between calculated halfwidths in the two branches obtained from any theoretical method can be easily established:

$$qR(j,k) \approx qP(j+1,k). \tag{6}$$

As shown in Fig. 3, within the experimental uncertainty, the measurements of Rinsland et al. [3] also confirm Eq. (6).

The weak or negligible vibrational dependence of both the rotational and molecular parameters leads to another consequence: a negligible vibrational dependence of the relaxation matrices. Therefore, calculations performed in the $\nu_4$ band can be applied to the analysis of the pure rotational band (see Secs. III-3 and III-4).

## 3. Results and discussions

Before presenting our results, we would like to point out that, due to the $CH_3CN$ molecule's large dipole and quadrupole moments, the interactions, especially in the $CH_3CN$—$N_2$ system, are very strong. When evaluating the matrix elements of *exp(-$S_2$)* (Eq. (3)), we encountered larger positive eigenvalues of the -$S_2$ matrix at short collisional distances, leading to divergence in the calculations. To prevent this blowout problem, we adopted a method we had previously developed to enforce the sufficient condition of the positive definite matrix on the -$S_2$ matrix [10]. Interested readers can refer to our earlier work for further details.

### 3.1. Calculated $N_2$-broadened halfwidths in the qR, qQ, and qP branches

We have performed extensive calculations at $T = 296$ K for $N_2$-broadened halfwidths of $CH_3CN$ lines in the $\nu_4$ band. Our calculations cover all three branches: qR(j,k), qQ(j,k), and qP(j,k), covering k values from 0 to 9 (or 1 to 10 for the qQ branch) and j values from the minimum to 46. Three different formalisms (i.e., MRB, RRB, and RRB with LM) have been used in these calculations. The results of our computations in the qR, qP, and qQ branches are presented below.

As shown in Fig. 4, the MRB method significantly overestimates the halfwidth in the qR branch when compared to the measurements. Incorporating LC using the RRB approach leads to a substantial reduction in the calculated halfwidths. However, even after having these LC reductions, the calculated halfwidths with RRB still significantly surpass the measured values. Finally, by using the latest method (i.e., RRB with LM) where both LC and LM are considered, the calculated halfwidths are significantly reduced further and very closely match the measurements.

At this stage, we would like to provide detailed analysis and

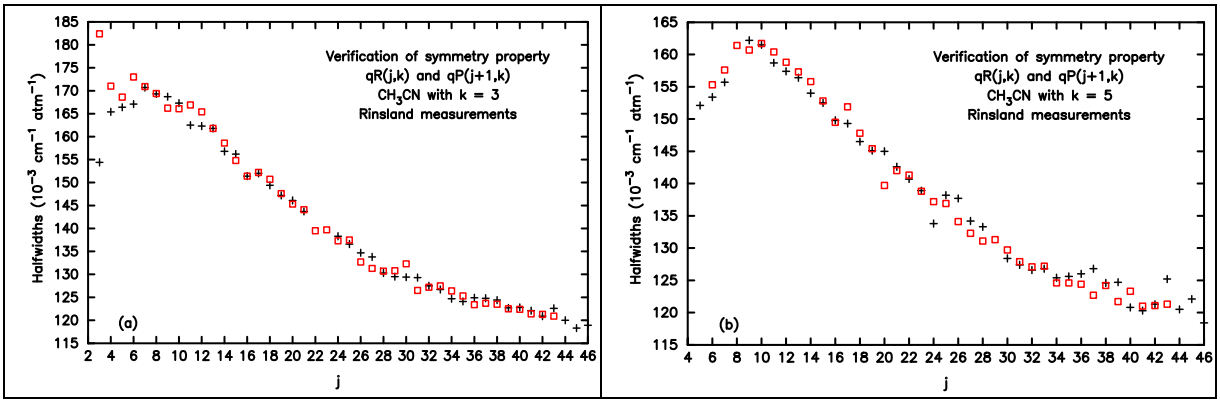


**Fig. 3.** Verification of the symmetry property qR(j,k) = qP($j$ + 1,k) for the $N_2$-broadened halfwidths with $k = 3$ and $k = 5$ measured by Rinsland et al. These are shown in panels (a) and (b), respectively. The halfwidths of qR(j,k) are represented by the black + symbols and the halfwidths of qP($j$ + 1,k) are represented by the red □ symbols.

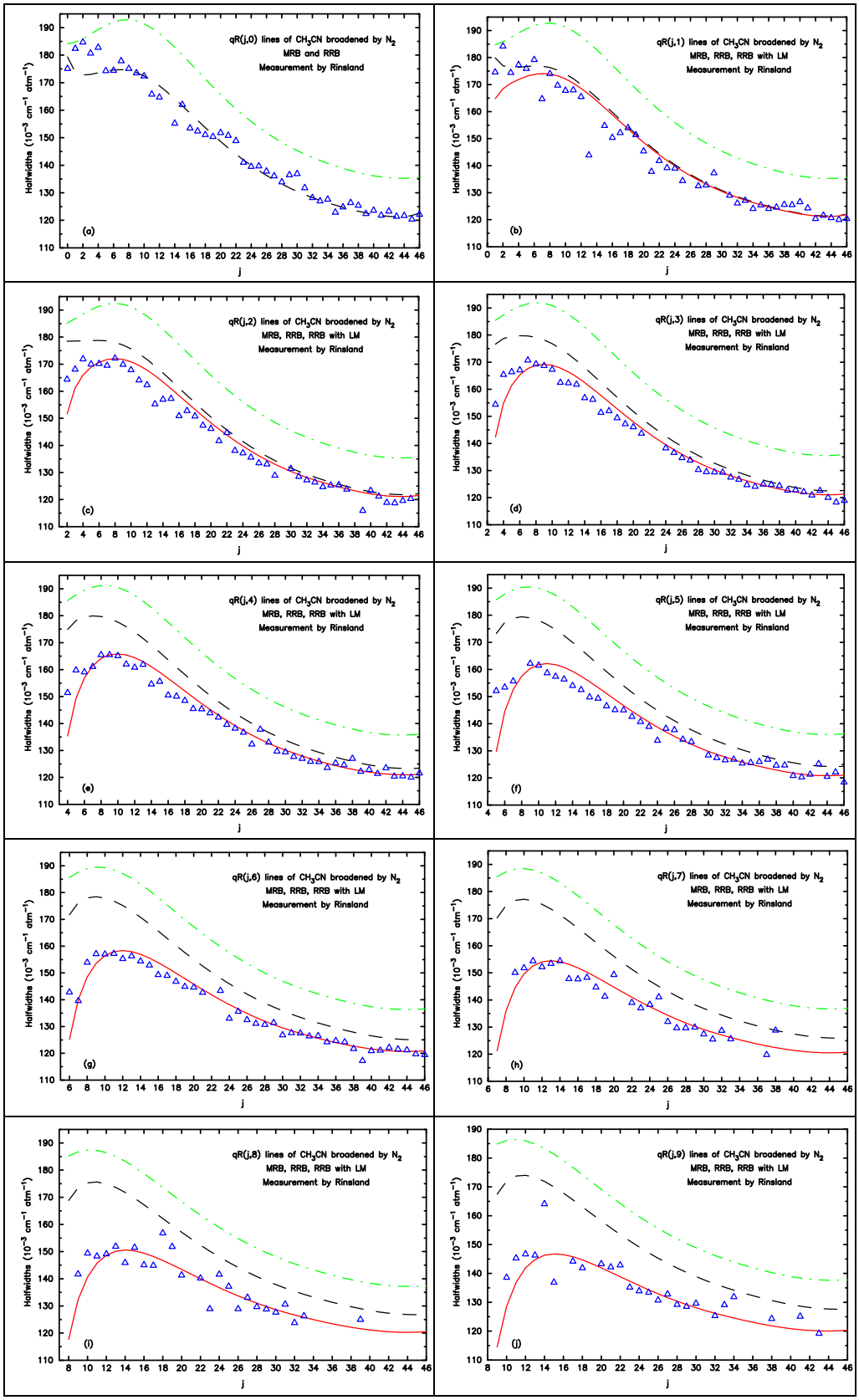


**Fig. 4.** The $N_2$-broadened halfwidths of the qR(j,k) lines for $k = 0, 1, \ldots, 9$ are presented in ten plots, labeled (a) through (j), respectively. These theoretically calculated values are obtained using the MRB method (green dotted dash), the RRB method (black dashed), and the RRB with LM method. For $k = 0$, since the doublets do not exit, only the first two methods are applied. Additionally, the measured $N_2$-broadened halfwidths by Rinsland et al. [3] are represented by the symbol Δ.

explanation for these two reductions. By using the same notations for the three methods to represent the corresponding calculated halfwidths, the first reduction is defined as (MRB-RRB)/MRB and the second one is defined as [RRB-(RRB with LM)]/RRB (i.e., W(1,2)/W(1,1)). In Fig. 5, for the qR branch, we present these two reductions as a function of j and k.

We emphasize that both reductions defined above originate from the same source: the non-diagonality of the $-S_2$ matrix. When calculating the W matrix using Eq. (3), a diagonalization procedure is introduced to evaluate the matrix elements of $exp(-S_2)$. This procedure completely leads to two different matrix element distributions of $-S_2$ and $exp(-S_2)$ (consequently, the W matrix itself). As a result, in addition to the off-diagonal matrix elements of $-S_2$ whose magnitudes can be well predicted from CSF(1), this diagonalization procedure may also play a critical role in determining the reductions.

First, let us analyze the first reduction. As shown in Fig. 5(a), the first reduction varies within 3% to 10% and it exhibits complex variation as the values of j and k change. As explained above, RRB involves the diagonalization procedure, whereas MRB does not. This difference suggests that the diagonalization procedure is responsible for the complex variation observed in the first reduction. The distinct variation behavior for $k \leq 2$, compared with higher k values, is due to an edge effect in the diagonalization procedure.

Concerning the second reduction of W(1,2)/W(1,1), we note that it becomes zero for $k = 0$ because the corresponding double does not exit. As shown in Fig. 5(b), the variation pattern with respect to j and k is well organized and it closely resembles CSF(1) shown in Fig. 2(a). Since both W(1,2) and W(1,1) are obtained following the diagonalization procedure, the effects of this procedure on the second reduction are canceled out. As a results, the variation is mainly determined by CSF(1). More specifically, the magnitude of the second reduction increases as k increases, especially for lines with the minimum j values (i.e., $j = k$). For a specified k value, the magnitude varies significantly with j. The maximum always occurs at the minimum j (i.e., $j = k$) and can reach as high as 32% for $k = 9$. In contrast, for the $j = 46$ line, the reduction becomes small or even negligible, particularly for small k values. Finally, by comparing Fig. 5(a) and 5(b), one can conclude that the second reductions is more significant than the first one.

We now present our results for the qQ branch. Theoretical calculations are performed similarly to those for the qR branch. However, it is worth mentioning that measuring individual halfwidths in this branch is nearly impossible due to the congestion of the spectra. As a result, measured halfwidths are not available. Instead, we compare our calculated halfwidths with the air-broadened data listed in HITRAN 2008. To convert these air-broadened values to $N_2$-broadened ones, they are multiplied by a factor of 1/0.93, as used in HITRAN 2008.

In Fig. 6, the explanations for the calculated $N_2$-broadened halfwidths of the qQ(j,k) lines using the three methods are similar to those for the qR branch and are therefore not repeated here. In this case, compared to the converted air-broadened data from HITRAN 2008, our results derived from the RRB with LM method also show very good agreement.

Next, we analyze the two reductions in the qQ branch and present their variation profiles in Fig. 7(a) and 7(b). The analysis and explanation of these reductions in the qQ branch are similar to those in the qR branch and are therefore not repeated here. However, it is worth noting that, in general, the reductions in the qQ branch are stronger than those in the qR branch, particularly for high k values. The maximum reduction, occurring at $j = k = 10$, can reach as high as 43%. As mentioned earlier, this is due to the higher magnitudes of CSF(1) in the qQ branch compared to those in the qR branch as shown in Fig. 2(a) and 2(b). In addition, as shown in Fig. 7(a), due to the edge effect, a distinct variation in the first reduction behavior occurs only for $k = 1$, unlike the three occurrence for $k = 0$, 1, and 2 in the qR branch. This difference may result from the fact that, compared to the qR branch, the inter-doublet off-diagonal elements of $-S_2$ in the qQ branch become less significant.

### 3.2. The j and k dependencies of calculated $N_2$-broadened halfwidths

**A. The j dependence in the qR, qQ, and qP branches**

For the j dependence of halfwidths in the qR branch, as shown in Fig. 8(a), except for $k = 0$ where the doublets do not exist, all other halfwidths increase quickly from their minimum j values (i.e., $j = k$) until reaching their maxima. The position of these maxima shifts to higher j values as k increases. After peaking, the halfwidths decrease at varying rates. Beyond $j > 36$, their variations with respect to j become smaller or even negligible.

For the j dependence of the qQ(j,k) lines shown in Fig. 8(b), compared to the qR(j,k) lines, all variation patterns with j are similar to those of the qR(j,k) lines with $k \neq 0$. However, the magnitudes at their minimum $j = k$ decrease more quickly as k increases compared to those of the qR(j,k) lines. This is due to the stronger magnitudes of CSF(1) in this branch, as mentioned earlier.

Note that due to the symmetry of $qP(j + 1,k) = qR(j,k)$, we do not present a figure showing the j dependence of the qP(j,k) lines. This figure would be identical to Fig. 8(a), except for shifting all the curves by one unit along the j axis.

**B. The k dependence of the qR, qQ, and qP branches**

As shown in Fig. 9(a), which includes lines with $1 \leq j \leq 18$, the halfwidths decrease as k increases. The rate of decrease with respect to k slows down as j increases. For $j \geq 12$, the curves become progressively flatter. In contrast, Fig. 9(b), which covers lines with $19 \leq j \leq 36$, shows

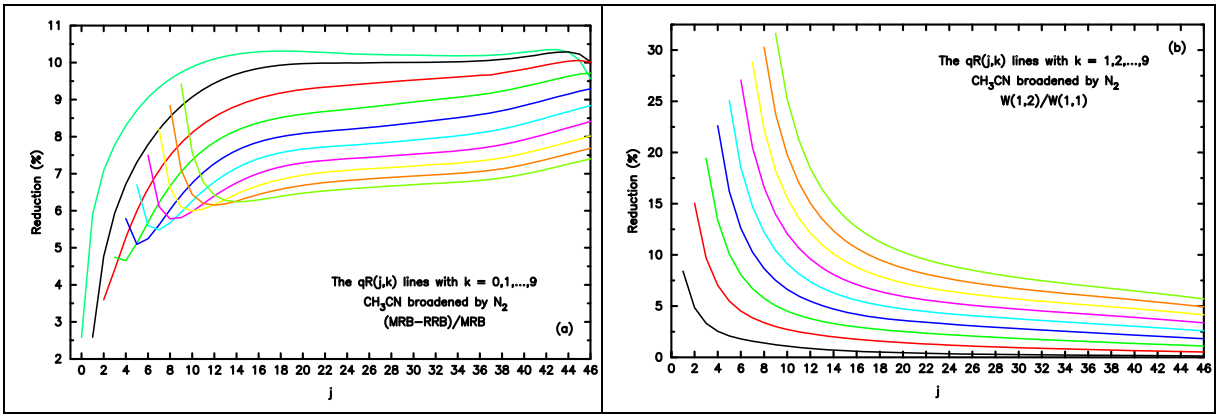


**Fig. 5.** Calculated first and second reductions of the qR(j,k) branch as functions of j and k in (a) and (b), respectively. For the first reduction, k values range from 0 to 9, while for the second reduction, k values range from 1 to 9. Different colors indicated the various k values. Additionally, since each of the k curves starts from $j = k$, this feature helps to differentiate them.

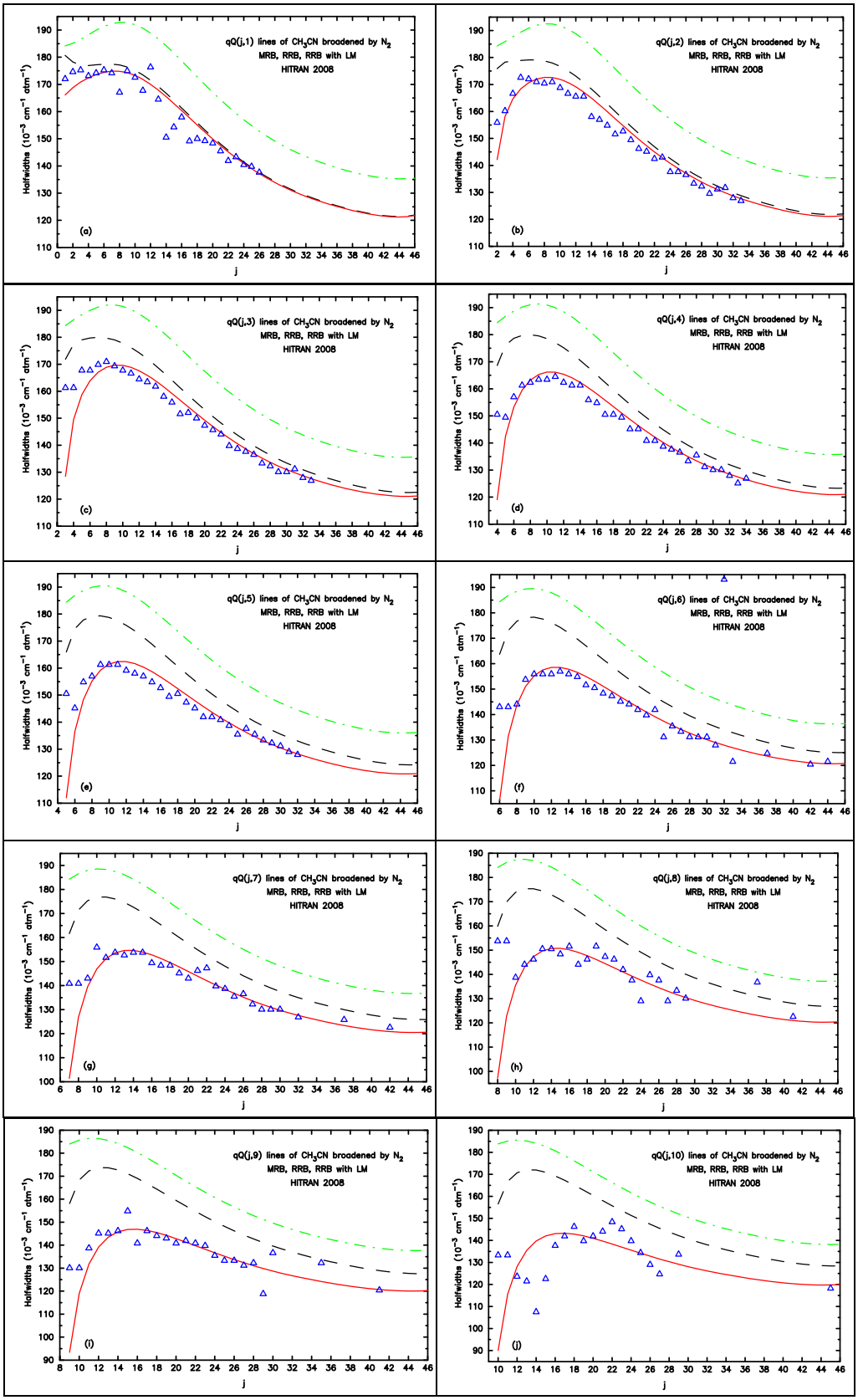


**Fig. 6.** The same as Fig. 4 except for the qQ(j,k) lines with k values range from 1 to 10. Besides, the air-broadened data listed in HITRAN 2008 are converted to the $N_2$-broadened ones by multiplying a factor of 1/0.93, and are presented by the symbol Δ.

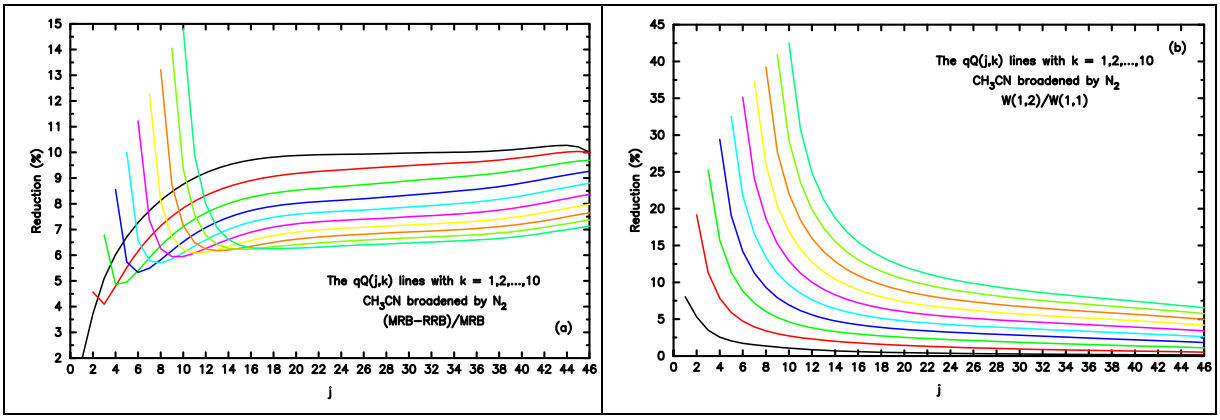


**Fig. 7.** The same as Fig. 5 except for the qQ(j,k) branch. Because the qQ(j,0) lines do not exit, the k values considered range from 1 to 10.

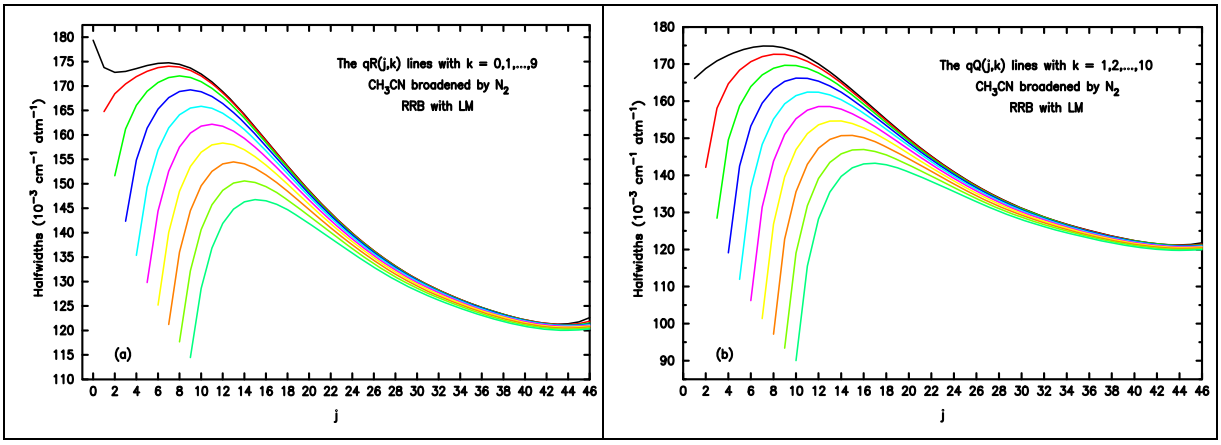


**Fig. 8.** The calculated halfwidths of the qR(j,k) and qQ(j,k) lines are shown as a function of j in (a) and (b), respectively. For qR(j,k), k values range from 0 to 9, while for qQ(j,K), k values range from 1 to 10. Different colors are used to distinguish the ten k values. Additionally, since each of the k curves starts from $j = k$, this feature helps to differentiate them. The calculations are based on the RRB with LM method.

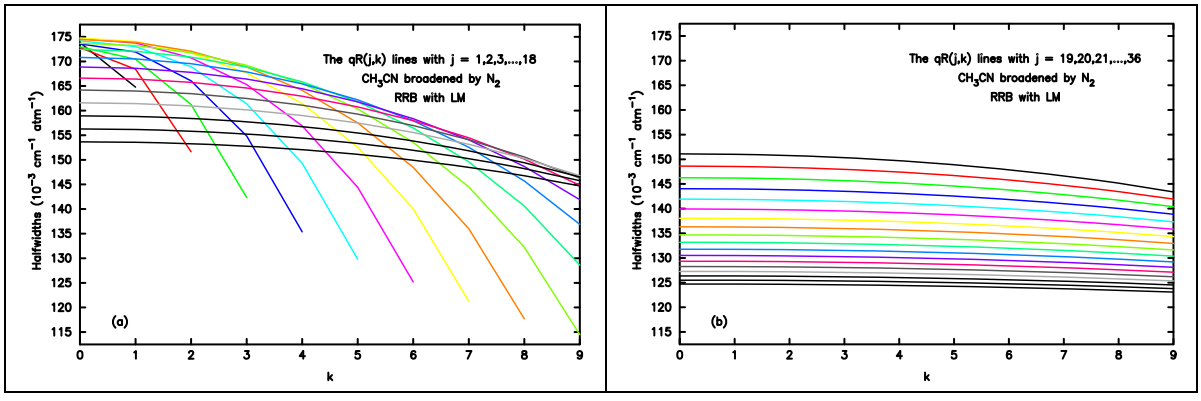


**Fig. 9.** As a function of k, the calculated halfwidths of the qR(j,k) lines for j values ranging from 1 to 18 and from 19 t0 36 are presented by solid curves in (a) and (b), respectively. Different colors distinguish the eighteen j values in each of these plots. The calculations are based on the RRB with LM method. A helpful hint for distinguishing the lines: in Fig. 9(a), for the lines with $j < 9$, the curves are truncated at $k = j$. Meanwhile, for the line with $j \geq 9$, the magnitudes of the lines at $k = 0$ decrease as j increases.

that the curves representing the halfwidths for these lines are relatively flat, and their magnitudes decrease as j increases.

For lines with $j > 36$, the calculated halfwidths in the qR branch exhibit no significant dependence on j and k. Therefore, they are not presented here.

In general, the explanations presented above for the qR branch also apply to the qQ branch and will not be repeated. However, one noteworthy feature is that, as shown in Fig. 10(a), for lines with $j \leq 9$, their minimum values, occurring at $k = j$ (i.e., at their truncation points), are smaller when compared to those in the qR branch shown in Fig. 9(a). This difference is attributed to the stronger CSF(1) of the qQ branch.

Additionally, due to the symmetry of qP($j + 1$,k) = qR(j,k), we do not

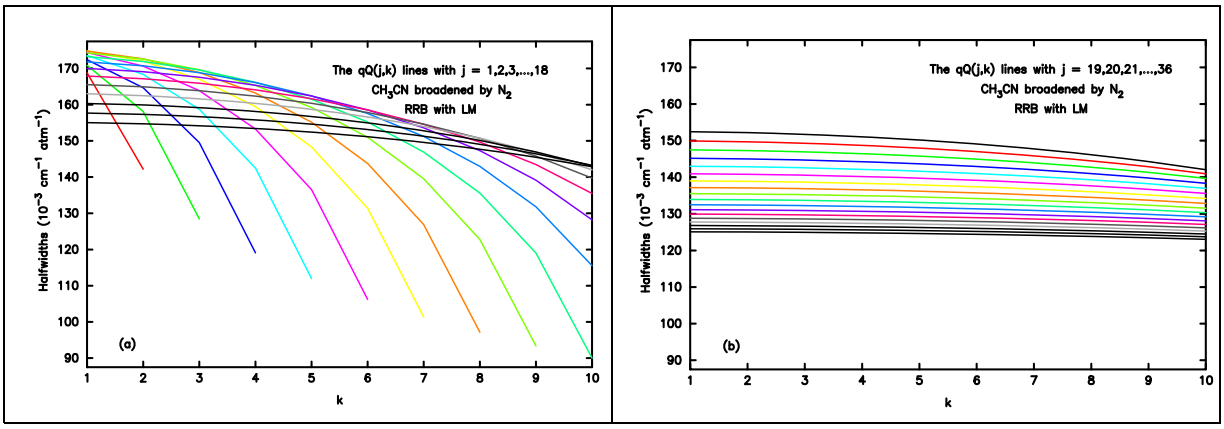


**Fig. 10.** The same as Fig. 9 except for the qQ(j,k) branch.

present figures showing the k dependence of the qP(j,k) lines. These figures would be identical to those of the qR(j,k) branch except for relabeling j as $j+1$. Finally, we note that the main features of the j and k dependencies shown in Figs. 8-10 are similar to those derived by Dudaryonok et al. using their semi-empirical method (see Fig. 1 of Ref. [2]).

### 3.3. Calculated $O_2$- and air-broadened halfwidths in the qR, qQ, and qP branches

Usually, air-broadened halfwidths are derived from $N_2$- and $O_2$-broadened halfwidths, by assuming a standard air composition of 79% $N_2$ and 21% $O_2$ and using a formula:

$$\gamma_{air} = 0.79\ \gamma_{N_2} + 0.21\ \gamma_{O_2} \tag{7}$$

To the best of our knowledge, no systematic measurements of $O_2$-broadened halfwidths are available. Previously, Fabian et al. reported $N_2$- and $O_2$-broadened halfwidths for the qR(4,k) and qR(5,k) manifolds (with $k$ = 0, 1, …, j) in the mmW region. The average ratio of $O_2$-broadened to the $N_2$-broadened halfwidths was found to be 0.67. According to Eq. (7), this implies that the ratio of air-broadening to $N_2$-broadending (i.e., the conversion factor) is 0.93, As mentioned above, this value was used in the development of the HITRAN 2008 database.

We performed calculations to derive the $O_2$-broadened halfwidths in the qR and qQ branches only. As explained previously, calculations for the qP branch are unnecessary. We then theoretically derive the air-broadened halfwidths in these branches using Eq. (7), with the results presented in Figs. 11 and 12, respectively. Additionally, we easily determined the value of the average conversion factor, which is 0.91 and closely matches Fabian's measured value of 0.93.

As shown in Fig. 11, our calculated air-broadened halfwidths in the qR branch derived from Eq. (9) match the HITRAN data pretty well. However, it is worth mentioning that as shown in Fig. 11(j), the qR(j,9) data listed in HITRAN 2008 are wildly scattered, indicating possible errors.

As shown in Fig. 12, our calculated air-broadened halfwidths for the qQ branch also agree well with the HITRAN data. Similar to the qR branch, the HITRAN data for high k values appear to be increasingly scattered. The higher the k value, the greater the scattering. This suggests that some errors may be present in certain lines.

Here, we would like to briefly discuss the conversion factor from $N_2$- to air-broadening. Based on our previous theoretical studies of the $CH_3F$ and $CH_3I$ molecules, our predicted values for these two molecules are 0.91 and 0.95, respectively. On the other hands, in developing HITRAN 2008, values of 0.90, 0.96, 0.96, and 0.93 were used for $H_2O$, $CH_3Cl$, $CH_3Br$, and $CH_3CN$ molecules [5]. From a theoretical standpoint, it is understandable that different molecules have different conversion factors due to variations in their molecular parameters and the different interactions they are involved in.

Furthermore, the fact that our theoretical calculations, without any adjustments, agree very well with Rinsland's measurements in the qR and qP branches not only validates the applicability of our formalism, but also confirms the reliability of Rinsland's data. In fact, our current study serves as strong support and provides theoretical explanations for their measurements. On the other hand, for the qQ branch, where Rinsland's measurements are not available, our theoretical results match the adjusted HITRAN values very well, demonstrating the reliability of the air-broadened data in HITRAN 2008 and the applicability of the conversion factor 0.93. Since new comprehensive measurements are unlikely to become available in the coming years, we hope that Rinsland's measurements, along with the conversion factor 0.93, will continue to serve as a valuable source for the development of the next version of HITRAN. Recently, from the HITRAN news posted in Oct. 2024, we were pleased to learn that the HITRAN committee accepted our suggestion to retain the conversion factor 0.93 in future updates to the $CH_3CN$ line list.

### 3.4. Temperature dependence of the $N_2$-broadened halfwidths

We have previously investigated the temperature dependence of the halfwidths for similar molecules, such as $CH_3F$ [13] and CH3Br [14]. In the present study, following the conventional approach, we use a power law to model the variation of halfwidths with temperature:

$$\gamma(T) = \gamma(T_0)\left(\frac{T_0}{T}\right)^N, \tag{8}$$

where $T_0$ = 296 K and $N$ is the temperature exponent.

For $CH_3CN$, only one measurement of the temperature dependence of an $N_2$-broadened halfwidth has been reported, limited to the qR(11,3) and qR(12,3) transitions in the pure rotational band [1]. For these lines, extensive measurements were performed over a range of temperatures from 235 K to 350 K and the temperature exponent $N$ = 0.718 was derived.

In Fig. 13, we present samples of the theoretical calculations for $N_2$-broadened halfwidths at $T$ = 250, 280, 310, and 340 K for the qR(j,3) lines. An additional sample at $T$ = 296 K can be found in Fig. 4(d).

Based on these theoretical results, we derived the temperature exponent $N$ by applying a least square procedure to fit Eq. (8). The results are presented in Fig. 14. The $N$ values obtained from the three methods show only slight differences. However, as illustrated in Fig. 14, the calculated $N$ values vary significantly depending on the line of interest. For the qR(11,3) and qR(12,3) lines, our corresponding $N$ values derived from the RRB with LM method are 0.752 and 0,727, respectively, which are closer to Colmont's measured value of 0.718. It is

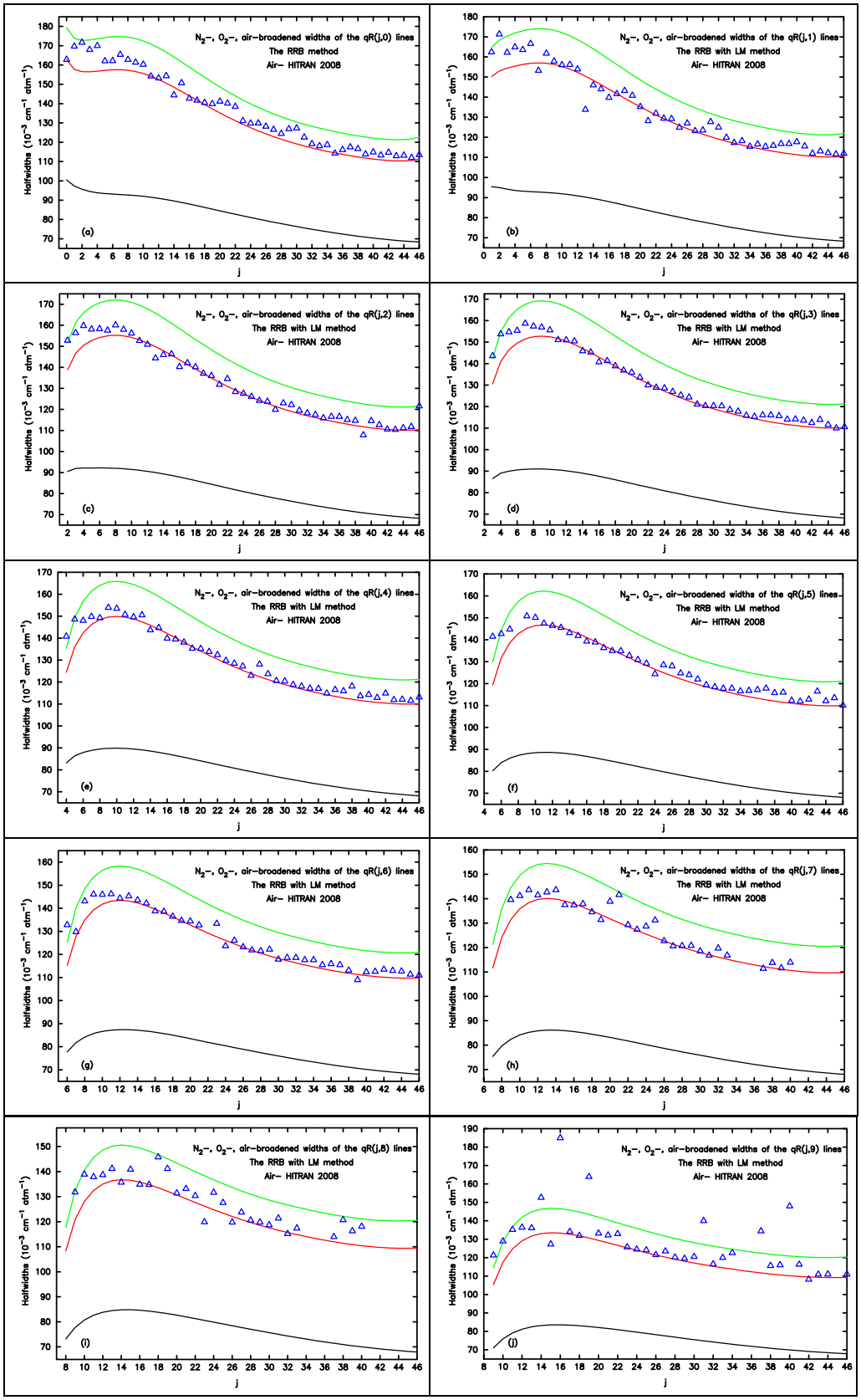


**Fig. 11.** Calculated $N_2$-, $O_2$-, and air-broadened halfwidths of the $CH_3CN$ lines in the qR(j,k) branch for k values ranging from 0 to 19 and j values from k to 46 using the RRB with LM method. These values are represented green, black and red lines, respectively. Additionally, the air-broadened halfwidths listed in HITRAN 2008 are presented by Δ.

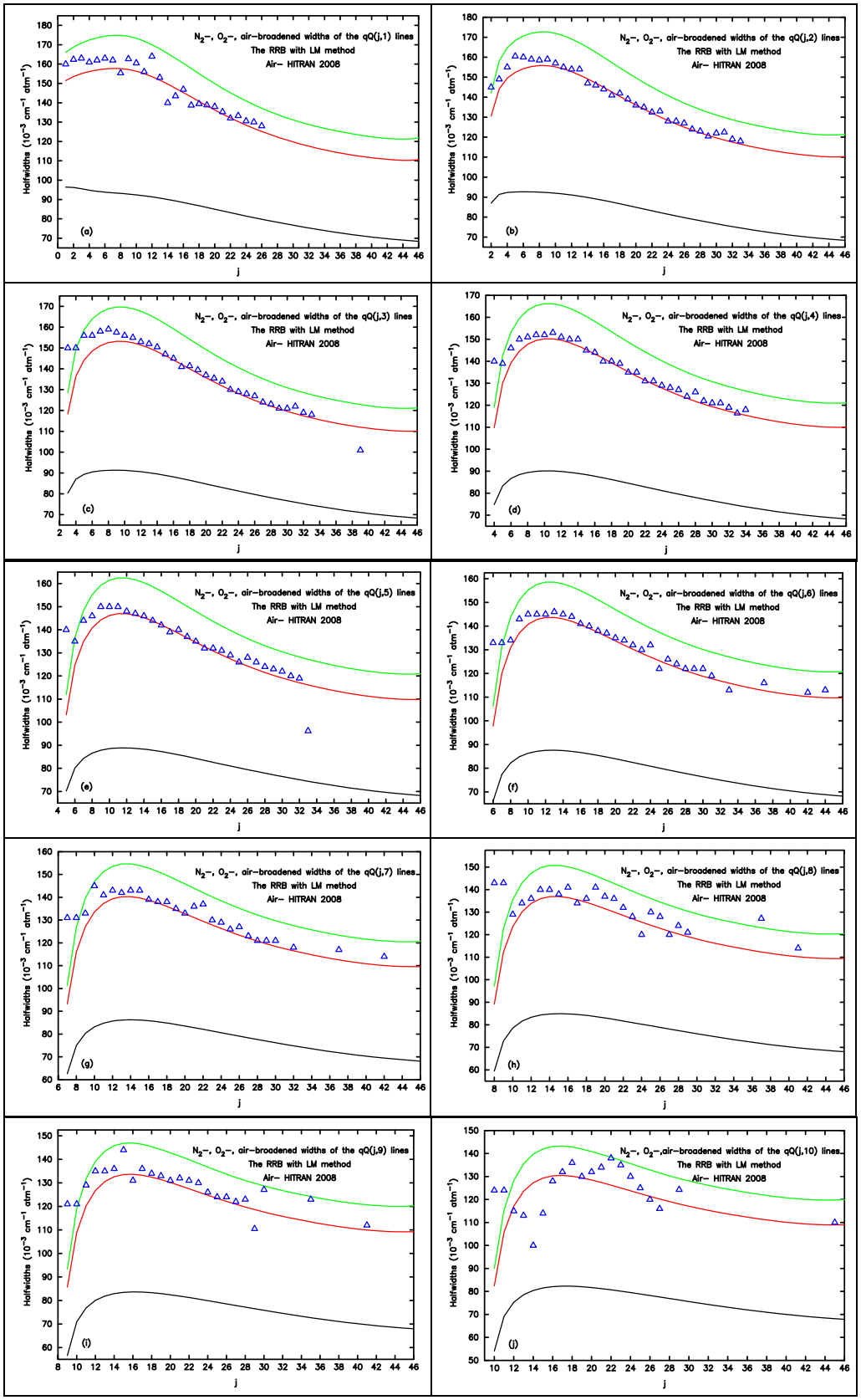


**Fig. 12.** The same as Fig. 11 except for the qQ(j,k) lines and k values range from 1 to 10.

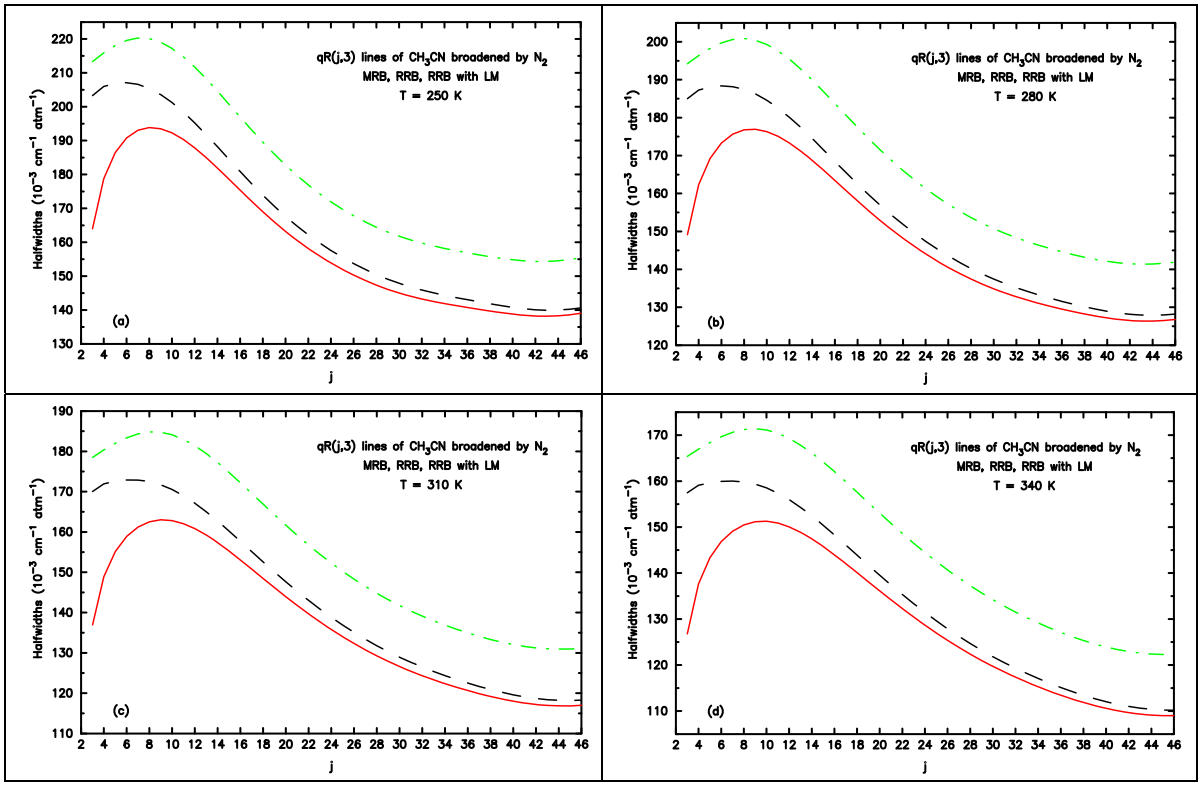


**Fig. 13.** The halfwidths of the qR(j,3) lines for $T = 250$, 280, 310, 340 K are presented in four plots, labeled (a) through (d), respectively. These values are obtained through the application of the MRB (green dotted dash), RRB (black dashed), and RRB with LM (red solid) methods.

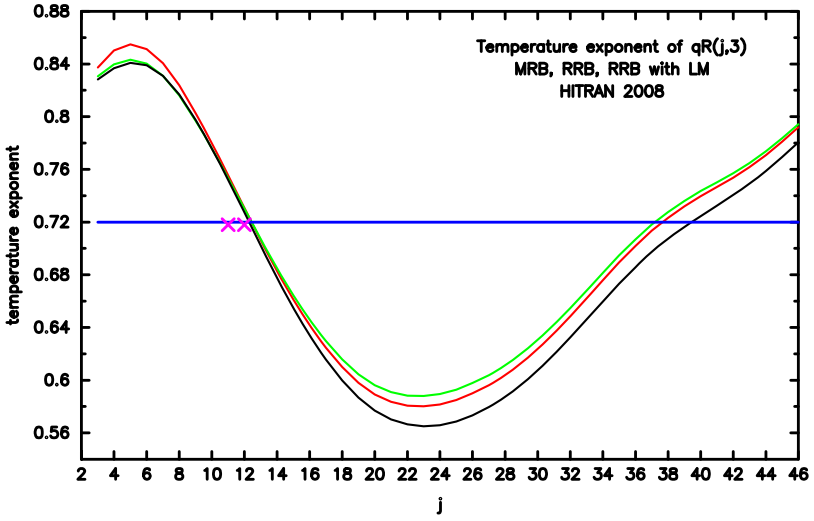


**Fig. 14.** Values of the temperature exponent $N$ obtained from the three models: MRB (black), RRB (green), and RRB with LM (red) are shown. The $N$ value listed in HITRAN 2008 ($N = 0.72$) is represented by a blue line. Additionally, two measured $N$ values (both 0.718) for the qR(11,3) and qR(12,3) lines, as reported by Colmont et al. [1], are indicated by magenta crosses (×).

noteworthy that their experimental $N_2$-broadened halfwidths for both these lines at $T = 296$ K are 160.9 (in the units of $10^{-3}$ $cm^{-1}atm^{-1}$), compared to Rinsland's measured values of 162.5 and 162.3, as well as our theoretical values of 167.9 and 166.4 for these two lines.

At this stage, we would like to point out that even when using "a rather low value of the quadruple moment of $N_2$", the theoretically calculated halfwidths derived from the RB formalism by Colmont et al. are 176.7, which is much larger than their measured values. This discrepancy is why they claimed that the RB method is not applicable to the $CH_3CN$—$N_2$ system, which involves a strong dipole and quadruple interaction.

During the development of HITRAN 2008, due to the lack of measurements for the temperature dependence of the air-broadened halfwidth and the availability of measured $N$ values only for two $N_2$-broadened $CH_3CN$ lines [1] indicated in Fig. 14, the default $N$ for all lines was set to 0.72. We believe that accurately modeling the temperature dependence of halfwidths will require incorporating the line dependence of $N$ into the HITRAN database. In the absence of experimental values, our current results could serve as a useful alternative.

For a detailed discussion on the physical origin of this rotational

dependence, the reader is referred to [13] and [25]. Finally, it is worth noting that the j dependence of our calculated *N* values is quite similar to those predicted by Dudaryonok et al. using their semi-empirical method within the same temperature range [2].

## 4. Conclusions

The present study is part of a series of works focused on the $N_2$-broadened halfwidths of $CH_3X$-species. Our study comprises three branches, encompassing a wide range of j and k quantum numbers. Similar to our previous studies, we have demonstrated that the isolated line approximation significantly limits the validity of the RB and MRB models. Specifically, when compared to experimental measurements, the calculated halfwidths using RB and MRB are significantly overestimated, indicating the need for a reduction. In our viewpoint, the shortcomings of RB and MRB stem from the disregard of the effects from LC and LM, which are incorrectly excluded due to the application of the isolated approximation. By considering the effect from LC, the RRB method leads to the first reduction in the calculated halfwidths, but they still remain overestimated. Subsequently, by using the RRB with LM method to consider both the effects from both LC and LM, the calculated halfwidths undergo the second reduction. We then compared our calculated halfwidths in the qR and qP branches derived from the RRB with LM method against the measurements of $N_2$-broadened halfwidths by Rinsland et al. Without any adjustments to the potential parameters, the agreement between our theoretical predictions show very good agreement with the experimental data.

## CRediT authorship contribution statement

**Q. Ma:** Writing – review & editing, Validation, Methodology, Investigation, Data curation. **C. Boulet:** Writing – original draft, Validation, Software, Methodology, Investigation, Formal analysis, Data curation, Conceptualization.

## Declaration of competing interest

The authors declare that they have no known competing financial interests or personal relationships that could have appeared to influence the work reported in this paper.

## Acknowledgement

One of the authors, Q. Ma, gratefully acknowledges the support received from the NASA Radiation Sciences Program, managed by Hal Maring. The research conducted in this study utilized resources provided by the National Energy Research Scientific Computing Center, which is supported by the Office of Science of the U.S. Department of Energy under Contract No DE-AC02-05CH11231.

During the preparation of this work the authors used ChatGPT in order to improve English. After using this tool/service, the authors reviewed and edited the content as needed and take full responsibility for the content of the publication.

## Data availability

Data will be made available on request.

## References

[1] Colmont J-M, Rohart F, Wlodarczak G, Bouanich JP. K-dependence and temperature dependence of $N_2$-, $H_2$- and He-broadening coefficients for the J = 12–11 transition of acetonitrile $CH_3C^{14}N$ located near 220.7 GHz. J Mol Spectrosc 2006;238:98–107.

[2] Dudaryonok AS, Lavrentieva NN, Buldyreva JV. $N_2$-broadening coefficients of $CH_3CN$ rovibrational lines and their temperature dependence for the Earth and Titan atmospheres. Icarus 2015;256:30–6.

[3] Rinsland CP, Malathy Devi V, Benner DC, Blake TA, Sams RL, Brown LR, Kleiner I, Dehayem-Kamadjeu A, Muller HSP, Gamache RR, Niles DL, Masiello T. Multispectrum analysis of the $\nu_4$ band of $CH_3CN$: positions, intensities, self- and $N_2$-broadening, and pressure-induced shifts. JQSRT 2008;109:974–94.

[4] Fabian M, Morino I, Yamada KMT. Analysis of the Line Profiles of $CH_3CN$ for the J = 5 ← 4 and J = 6 ← 5 Rotational Transitions. J Mol Spectrosc 1998;190:232–9.

[5] Rothman, et al. The HITRAN 2008 molecular spectroscopic database. JQSRT 2009; 110:533–72.

[6] Bykov AD, Lavrentieva NN, Sinitsa LN. Semi-empiric approach to the calculation of $H_2O$ and $CO_2$ line broadening and shifting. Mol Phys 2004;102:1653–8.

[7] Robert D, Bonamy J. Short range force effects in semiclassical molecular line broadening calculations. J Phys 1979;40:923–43.

[8] Cherkasov MR. Theory of relaxation parameters of the spectrum shape in the impact approximation. I-General consideration. JQSRT 2014;141:73–88.

[9] Buffa G, Tarrini O. Microwave radii in nonresonant spectra. Phys Rev A 1977;16: 1612–6.

[10] Ma Q, Boulet C. Theoretical study of $CH_3Cl$-$N_2$ line shapes in the $\nu_1$ band. Line mixing effects in QR doublets and QQk sub-branches. JQSRT 2021;273:107844.

[11] Boulet C, Ma Q. Line coupling and line mixing effects on calculated widths of symmetric top molecules with the k-degeneracy: a theoretical study of $N_2$-, $O_2$- and air-broadened lines of $CH_3I$. JQSRT 2022;288:108273.

[12] Ma Q, Boulet C. The j and k dependencies of the line coupling and line mixing effects: theoretical studies of the relaxation matrices of $N_2$-broadened $CH_3D$. JQSRT 2023;299:108504.

[13] Boulet C, Ma Q. The influence of line mixing on the j and k dependencies of halfwidths and temperature exponents in $N_2$-broadening coefficients of $CH_3F$ spectral lines. JQSRT 2023;310:108716.

[14] Ma Q, Boulet C. Branch dependence of halfwidths: theoretical analysis of $N_2$-broadened halfwidths of $CH_3Br$ in the $\nu_6$ band. JQSRT 2024;320:108972.

[15] Ma Q, Tipping RH, Boulet C. Modification of the Robert–Bonamy formalism in calculating Lorentzian half-widths and shifts. JQSRT 2007;103:588–96.

[16] Ma Q, Boulet C, Tipping RH. Refinement of the Robert-Bonamy formalism: considering effects from the line coupling. J Chem Phys 2013;139:034305.

[17] Green S. Rotational excitation of symmetric top molecules by collisions with atoms. II. Infinite order sudden approximation. J Chem Phys 1979;70:816–29.

[18] Boulet C, Ma Q, Thibault F. Line interference effects using a refined Robert-Bonamy formalism: the test case of the isotropic Raman spectra of $N_2$. J Chem Phys 2014; 140:084310.

[19] Ma Q, Boulet C, Tipping RH. Relaxation matrix for symmetric tops with inversion symmetry: line coupling and line mixing effects on $NH_3$ lines in the $\nu_4$ band. J Chem Phys 2017;146:134312.

[20] Ben-Reuven A. Impact broadening of microwave spectra. Phys Rev 1966;145:7–22.

[21] Ma Q, Boulet C. The relaxation matrix for symmetric tops with inversion symmetry. I. Effects of line coupling on self-broadened $\nu_1$ and pure rotational bands of $NH_3$. J Chem Phys 2016;144:224303.

[22] Troitsyna L, Dudaryonok A, Filippov N, Lavrentieva N, Buldyreva J. Oxygen- and air-broadening coefficients for the $CH_3I$ $\nu_6$ fundamental at room temperature. JQSRT 2021;273:107839.

[23] Bouanich JP, Blanquet G, Walrand J. Theoretical $O_2$- and $N_2$-Broadening Coefficients of $CH_3Cl$ Spectral Lines. *J Mol* Spectrosc 1993;161. *416-26*.

[24] Ma Q, Boulet C, Tipping RH. Two dimensional symmetric correlation functions of the *S* operator and two dimensional Fourier transforms: considering the line coupling for P and R lines of linear molecules. J Chem Phys 2014;140:104304.

[25] Hartmann JM, Taine J, Bonamy J, Labani B, Robert D. Collisional broadening of rotation-vibration lines for asymmetric-top molecules. II. $H_2O$ diode laser measurements in the 400–900 K range; calculations in the 300–2000 K range. J Chem Phys 1987;86:144–56.